RSC Advances

PAPER

View Article Online
View Journal | View Issue

Cite this: *RSC Adv.*, 2020, **10**, 18526

Electrochemical sensor using poly-(L-cysteine) functionalized CuO nanoneedles/N-doped reduced graphene oxide for detection of lead ions†

Suling Yang, *[ab] Panpan Liu,[ab] Yuxin Wang,[ab] Ziling Guo,[ab] Ruifan Tan[ab] and Lingbo Qu[abc]

A highly sensitive and selective electrochemical sensor modified with poly-(L-cysteine)/CuO nanoneedles/N-doped reduced graphene oxide (L-Cys/NN-CuO/N-rGO) has been prepared for the testing of trace Pb^{2+}. The electrochemical performance of this proposed sensor was investigated using electrochemical impedance spectroscopy (EIS). Based on the excellent electrochemical properties of NN-CuO/N-rGO as well as the specific complexation of natural substance L-cysteine with Pb^{2+}, the L-Cys/NN-CuO/N-rGO was applied as a voltammetric biosensor for the determination of trace Pb^{2+} at pH 5.0. Under the optimum experimental conditions, the voltammetric peak current was linear with the Pb^{2+} concentration over the range from 0.001 to 5.0 nM and 5.0 to 1000 nM, respectively, with a low detection limit for Pb^{2+} concentration on the biosensor of 8.0×10^{-5} nM (S/N = 3). The significant sensitivity, selectivity, and electron conductivity of this L-Cys/NN-CuO/N-rGO modified electrode have also been studied. The specific detection of Pb^{2+} in water samples was also carried out.

Received 8th April 2020
Accepted 7th May 2020

DOI: 10.1039/d0ra03149f

rsc.li/rsc-advances

1. Introduction

Transition heavy metal ions, especially lead ions (Pb^{2+}) can accumulate in the human body, which results in sub-toxic exposure levels to toxic levels over a period of accumulation.[1,2] The lead ion has been classified as a carcinogenic ion by the WHO International Agency for Research on Cancer. According to the exposure time and the concentration levels of Pb^{2+}, the long-term exposure to low concentrations of Pb^{2+} in the environment may lead to adverse health problems, which would increase the risk of cancer. Thus, a highly specific and sensitive method for the analysis of Pb^{2+} in food and the human environment has received more attention. Generally speaking, electrochemical methods have many advantages, such as cheap and portable equipment, simple operation, as well as high specificity and sensitivity. In recent years, electrochemical techniques have been developed for the analysis and detection of Pb^{2+}. Various types of electrochemical sensor have been constructed for the determination of trace metal contamination.

Graphene has a two-dimensional nanostructure and attractive properties, for instance, large surface area, high electron conductivity and excellent mechanical stability,[3] which makes it extensive applications, such as using as biosensors,[4] and electrochemical determination of heavy metal ions.[5] In addition, it has been clearly studied that graphene/metal oxide nanocomposites have showed more attractive properties in their promising applications than using a single graphene or nanometal oxide,[6–9] because the advantages of the two substances can be better displayed. So, it is a significative and attractive strategy that CuO nanomaterials are synthesized and grown on graphene sheets as the electrode material to fabricate electrochemical sensors. The prepared nanocomposite exhibits excellent synergistic effect of CuO nanomaterials and graphene compared with the sole substance.[9–11] Majumdar *et al.*[12] have successfully prepared CuO nanoparticles anchored on graphene surface for energy storage applications. Felix *et al.*[13] have fabricated graphene/CuO nanocomposites by electrode position method, and the CuO coated graphene served as a superior electrode material for non-enzymatic glucose detection. Moreover, the CuO nanoparticles doped onto graphene sheets not only can effectively stopping the aggregation of CuO nanoparticles and graphene, but also can maintain the electrochemical active sites of CuO nanoparticles. Therefore, the CuO/graphene nanocomposite is an interesting electrode material with enhanced electronic conductivity.

L-Cysteine, one of many important amino acids, is widely used in many medicines, food and biological tissue. Generally speaking, L-cysteine is one of the effective natural products to

[a]College of Chemistry and Chemical Engineering, Anyang Normal University, Anyang 455002, PR China. E-mail: yang_suling@163.com; Fax: +86 3722900040; Tel: +86 03722900040

[b]Henan Key Laboratory of New Opto-electronic Functional Materials, China

[c]College of Chemistry and Molecular Engineering, Zhengzhou University, Zhengzhou 450001, PR China

† Electronic supplementary information (ESI) available. See DOI: 10.1039/d0ra03149f

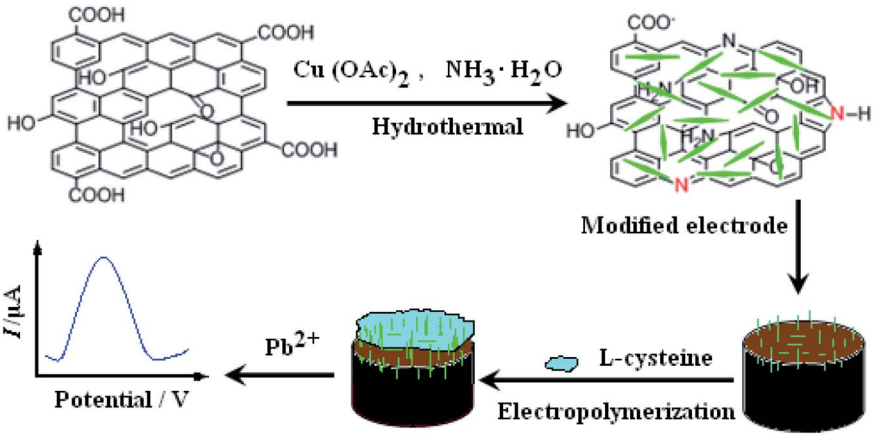

Scheme 1 The constructing process of the L-Cys/NN-CuO/N-rGO modified electrode.

treat lead in environment. It has come to be seen as a promising candidate for the poisoning treatment of lead in virtue of the chelating abilities of the chelating groups. As far as we know, Wang *et al.*[14] have presented the ultrathin CdSe nanoplatelets modified with either L or D-cysteine molecules to realize lead ion detection. Cheng *et al.*[15] have fabricated a biosensor by using L-cysteine-modified gold nanoparticles/nitrogen-doped graphene composite for lead determination. Zhou *et al.*[16] have reported an L-cysteine/graphene electrochemical sensors for determining lead ion. These reports have showed that L-cysteine, as a natural product, can form sensitive electrochemical sites on the surface of the sensor. Moreover, L-cysteine may identify Pb^{2+} in wastewater to produce stable complexes leading to pre-concentration purposes, and realize the detection of Pb^{2+}.

In this study, a nano-needle CuO/N-doped reduced graphene oxide nanocomposite was synthesized and used as electrode sensing material on the electrode. Subsequently, the nano-needle CuO/N-doped reduced graphene oxide modified electrode was covered with L-cysteine by using electropolymerization. The electrode constructing process is displayed in Scheme 1. To the best of our knowledge, it is the first time that nano-needle CuO/N-doped reduced graphene oxide nanocomposite and L-cysteine are bound together through preparing a sensor to research their unique synergistic effect for the electrochemical determination of Pb^{2+}. Electrochemical behaviors of Pb^{2+} on the prepared sensor were carefully studied and a sensitive square wave voltammetry (SWV) for Pb^{2+} detection was further established. The proposed method showed excellent electrochemical behaviors and could be employed for the detection of Pb^{2+} in real water samples.

2. Experimental

2.1. Reagent and apparatus

Graphene oxide (GO, 99 wt%) was purchased from Sigma-Aldrich. L-Cysteine (analytical reagent, purity ≥ 99.8%) in this study was obtained from Chinese Institutes for Food and Drug Control. All other chemicals, such as $PbNO_3$, $Cu(NO_3)_2 \cdot 3H_2O$, $Cu(Ac)_2 \cdot 3H_2O$, KNO_3, $K_3Fe(CN)_6$, $K_4Fe(CN)_6$, $NiSO_4 \cdot 7H_2O$, $Cd(NO_3)_2 \cdot 4H_2O$, and $Zn(NO_3)_2 \cdot 6H_2O$, were of analytical grade purity (purity ≥ 99.5%) and provided from Sinopharm Chemical Reagent Co., Ltd. Unless otherwise stated, the buffer solution is a 0.1 M KNO_3 (pH 5.0). The deionized water was used for all the experiments. And the used all solutions were deoxygenated by nitrogen. CuO nanoneedles/N-doped reduced graphene oxide (NN-CuO/N-rGO) was synthesized according to our former report.[17] Total solution volume used in Pb^{2+} detection tests was 10 mL in electrolytic cell.

All the electrochemical experiments were executed on a CHI660e electrochemical workstation (Shanghai Chenhua Instrument, China) with a conventional three-electrode system. The L-Cys/NN-CuO/N-rGO modified electrode was used as the working electrode. An Ag/AgCl and a platinum wire electrode were used as a reference electrode and auxiliary electrode, respectively. Scanning electron microscopy (SEM) was conducted on a JSM-6700F scanning electron microscope (Japan Electron Company, Japan).

2.2. Fabrication of the modified electrode

According to our former report,[17] NN-CuO/N-rGO and N-rGO were synthesized. NN-CuO/N-rGO modified carbon paste electrode (CPE) was prepared as follows: 0.8 g NN-CuO/N-rGO, 1.2 g graphite powder and a modest amount of silicon oil were mixed together and fully ground in an agate mortar. The resulting homogeneous paste was filled into one end of a glass tube ($d = 4$ mm) and the other end was inserted by a copper wire for electrical contact. So, NN-CuO/N-rGO/CPE was prepared. N-rGO/CPE was obtained by the similar process. CPE was also made by the same procedure without NN-CuO/N-rGO and N-rGO. The fresh prepared electrodes were polished carefully on a weighing paper just before use.

L-Cysteine was electro-polymerized on the prepared NN-CuO/N-rGO/CPE by cyclic voltammetry in the potential range of −0.8 to 2.0 V for 10 cycles at the scan rate of 0.1 mV s^{-1} in 1.0×10^{-3} M L-cysteine solution. After that, the L-Cys/NN-CuO/N-rGO/CPE was obtained. And then the electrode surface was cleaned with deionized water and N_2-dried.

3. Results and discussion

3.1. Characterization of the nanocomposites

The shape of the prepared materials was carried out by SEM (seen Fig. 1). Fig. 1a obviously revealed a wrinkled texture of N-

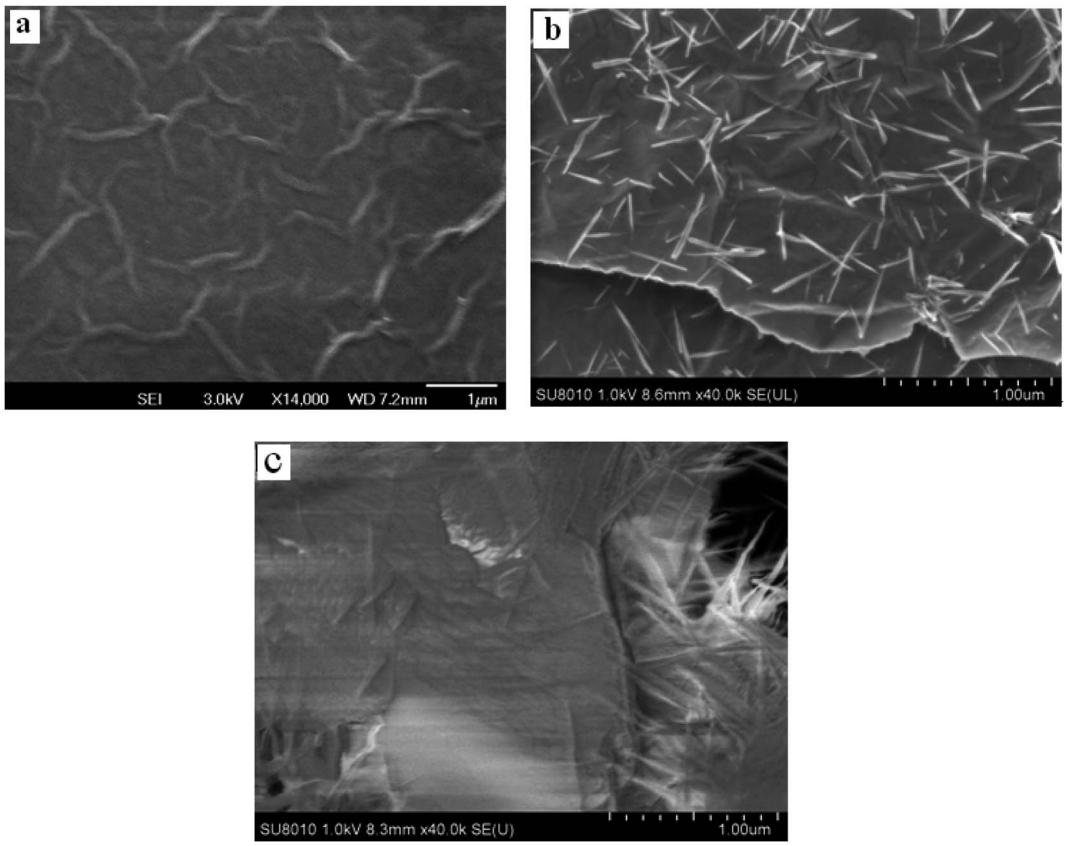

Fig. 1 SEM images of N-rGO (a), NN-CuO/N-rGO nanocomposite (b) and L-Cys/NN-CuO/N-rGO/CPE (c).

rGO planar sheets, showing that the essential structure of graphene was splendid existed. As can be seen from Fig. 1b, a great deal of nanoneedle-like CuO permeate the N-rGO planar sheets, and equally distributed on it with the wide size of about 20–100 nM and long size of about 0.5 μm. Fig. 1c shows finally electrode of L-Cys/NN-CuO/N-rGO/CPE. A thin film was covered on the electrode surface, showing the formation of electropolymerization of L-cysteine. Moreover, the electropolymerization process has not altered the CuO needle morphology. The formations of nanoneedle-like CuO maybe intensively increase the specific surface area of the as-prepared materials. This experimental result was consistent with our former report.[17] From the XPS (Fig. S1†) and EDS examinations (Fig. S2†), the elemental composition was confirmed the presence of C, O, N and Cu elements which have an uniform distribution within nanocomposite.

3.2. Electropolymerization of L-cysteine

As shown in Fig. 2, L-cysteine was electro-polymerized on the prepared NN-CuO/N-rGO/CPE by cyclic voltammetry in the potential range of −0.8 to 2.0 V at a scan rate of 0.1 mV s^{-1} in 1.0 × 10^{-3} M L-cysteine solution (0.1 M phosphate buffer solution, pH 6.86). During the first scan, there were two oxidation peaks, and the oxidation–reduction peak current increased with the increase of scanning times, which indicated that L-cysteine had been fixed on the electrode surface.[18] After the electropolymerization was completed, the electrode was washed with deoxygenated water. Compared with the NN-CuO/N-rGO/CPE, there was a layer of material with special luster on the electrode surface, which explained that the L-Cys/NN-CuO/N-rGO/CPE had been formed.

The effect of the thickness of the electro-polymerized film on the response current of Pb^{2+} was studied. Typically speaking, the film thickness can be easily adjusted by the number of cyclic scans. Initially, the current value of Pb^{2+} increased with increasing number of scan cycles. A maximum current value was obtained at 10 scan cycles, and then decreased with further increase of the scan cycle number. This reason can be possibly

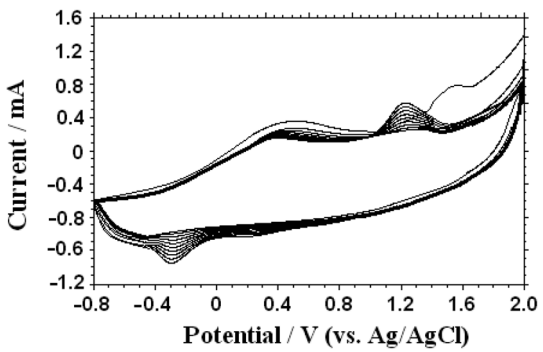

Fig. 2 Electro-polymerized process of L-cysteine on the prepared NN-CuO/N-rGO/CPE by cyclic voltammetry for 10 cycles at the scan rate of 0.1 mV s^{-1}.

explain that very thin films do not have enough active sites, whereas too thick films would block the electron transfer. Therefore, 10 cyclic scans were selected as the optimal condition to fabricate the electro-polymerized film on the electrode surface.

3.3. Electrochemical impedance studies

Electrochemical impedance spectroscopy (EIS) is an effective measure for proving the change of electrode interface. Generally speaking, the semicircle diameter equals to the electron transfer resistance (R_{et}). Fig. 3 showed the EIS of the NN-CuO/N-rGO/CPE (a), N-rGO/CPE (b), L-Cys/NN-CuO/N-rGO/CPE (c) and CPE (d) in 5.0 mM $Fe(CN)_6^{3-/4-}$ and 0.1 M KCl solution in the frequency range swept 10^5 to 0.1 Hz. The AC voltage amplitude was 5 mV, and the applied potential was 0.250 V. The Randles equivalence circuit model used to fit the experimental data was shown in the inset of Fig. 3, which included the ohmic resistance of the electrolyte (R_s), the electron transfer resistance (R_{et}), the double layer capacitance (C_{dl}), and Warburg impedance (Z_w). The bare CPE had a big semicircle diameter with a R_{et} value of 395.0 Ω. While the rGO/CPE and NN-CuO/N-rGO/CPE showed low R_{et} of 140.5 and 74.2 Ω, respectively, However, L-Cys/NN-CuO/N-rGO/CPE showed a R_{et} of 172.3 Ω, higher than the values of the rGO/CPE or NN-CuO/N-rGO/CPE. This phenomenon can be ascribed to the rGO nanosheets or NN-CuO/N-rGO in the electrode, but the L-cysteine layer obstructed the electron transport. The EIS demonstrated that the construction of each step had been successfully conformed.

The microscopic areas of the prepared modified-electrodes were obtained by cyclic voltammetry employing 1.0 mmol L^{-1} $K_3Fe(CN)_6$ as a redox probe in the 0.1 mol L^{-1} KCl electrolyte at different scan rates.[19,20] For a reversible process, the anodic peak current i_p is linear to $v^{1/2}$ as follows:

$$i_p = (2.69 \times 10^5) n^{3/2} A C_0 D_R{}^{1/2} v^{1/2}$$

where i_p refers to the anodic peak current, A the surface area of the electrode, v the scan rate and C_0 the concentration of

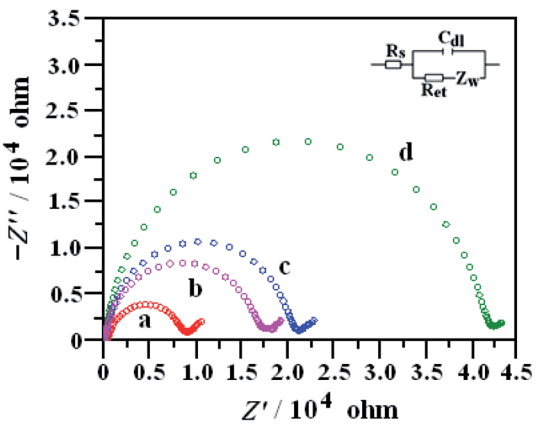

Fig. 3 Nyquist plots of the EIS the NN-CuO/N-rGO/CPE (a), N-rGO/CPE (b), L-Cys/NN-CuO/N-rGO/CPE (c) and CPE (d) in 5.0 mM $Fe(CN)_6^{3-/4-}$ and 0.1 M KCl solution in the frequency range swept 10^5 to 0.1 Hz at 0.25 V.

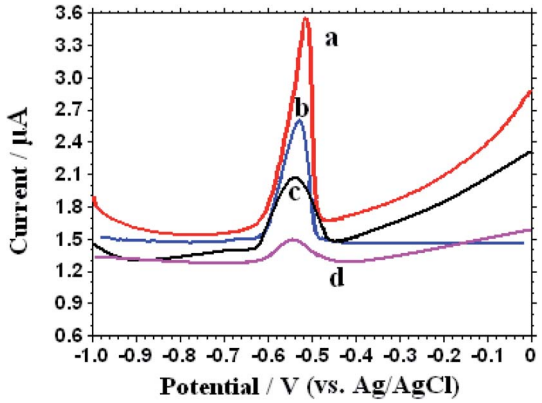

Fig. 4 Different SWVs of L-Cys/NN-CuO/N-rGO/CPE (a), NN-CuO/N-rGO/CPE (b), N-rGO/CPE (c) and CPE (d) in the presence of 1.0 μM Pb^{2+} in 0.1 M KNO_3 (pH 5.0).

$K_3Fe(CN)_6$. For 1.0 mmol L^{-1} $K_3Fe(CN)_6$, the electron transfer $n = 1$, the diffusion coefficient $D_R = 7.60 \times 10^{-6}$ cm^2 s^{-1}. Thus, from the slope of the i_p *vs.* $v^{1/2}$ relation, the microscopic areas of the N-rGO/CPE, NN-CuO/N-rGO/CPE and L-Cys/NN-CuO/N-rGO/CPE were calculated to be 0.9729 cm^2, 1.0738 cm^2, 1.0937 cm^2, respectively, which were great higher than the bare CPE (0.1256 cm^2). In combination with the EIS analysis, the electrochemically active surface area of the CPE, N-rGO/CPE, NN-CuO/N-rGO/CPE and L-Cys/NN-CuO/N-rGO/CPE were calculated to be 49.6, 136.7, 79.7 and 188.4 ohm cm^2.

3.4. Electrochemical behaviors of Pb^{2+} on different electrodes

The electrochemical features of 1.0 μM Pb^{2+} on different electrodes was studied through the square wave voltammetry (SWV) in 0.1 M KNO_3 (pH 5.0), which has been shown in Fig. 4. After electrochemical accumulation time for 250 s at an accumulation potential −0.6 V, frequency 15 Hz, and amplitude 25 mV, a well-shaped electrochemical stripping peak appears in the potential range from −0.48 to −0.60 V with different stripping peak current on different electrodes. An unobvious stripping peak current of Pb^{2+} was seen on the bare CPE at −0.52 V. In contrast, the peak current can be obviously enhanced on the NN-CuO/N-rGO and N-rGO modified electrodes because of the larger surface area and fast electron conductivity of the electrodes. It's interesting to see that the peak current remarkably increased after the introduction of L-cysteine on the NN-CuO/N-rGO modified electrode. The possible reason may be that L-cysteine can effective combine with Pb^{2+} and provide more enrichment sites for Pb^{2+} accumulation. All the experimental results showed that the interaction between analytical object of Pb^{2+} and L-Cys/NN-CuO/N-rGO has improved the electrochemical signal, and furnished a possibility for the selective recognition of Pb^{2+}.

3.5. Analytical conditions

In order to obtain the maximum efficacy of L-Cys/NN-CuO/N-rGO/CPE, some experimental conditions were optimized, such

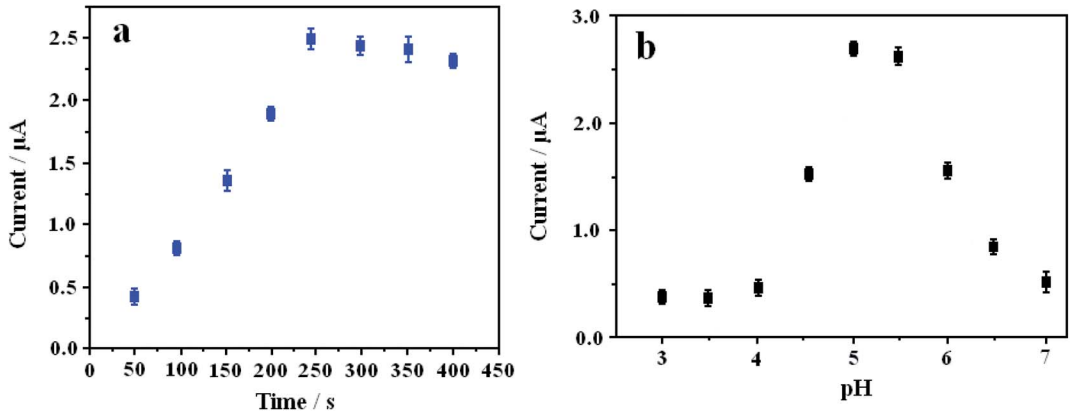

Fig. 5 Influences of different accumulation time of 1.0 μM Pb^{2+} in 0.1 M KNO_3 (pH 5.0) (a) and different pH in 1.0 μM Pb^{2+} in 0.1 M KNO_3 (b) on the striping peak current. Error bars are the standard deviation for three determinations.

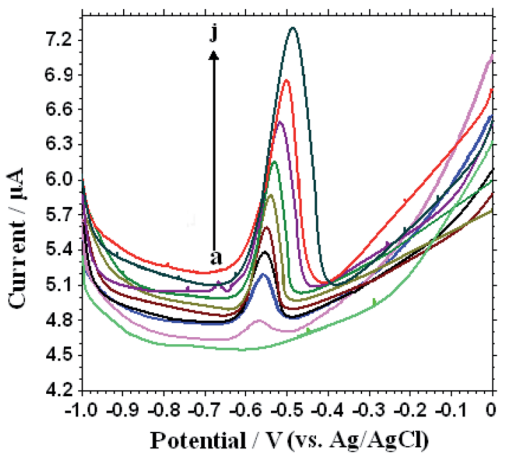

Fig. 6 SWV response of different concentrations of Pb^{2+} solution on the L-Cys/NN-CuO/N-rGO/CPE in 0.1 M KNO_3 (pH 5.0) (a → j): 0, 0.001, 0.08, 0.5, 1.0, 1.5, 2.2, 3.0, 4.0 and 5.0 nM.

as accumulation time for Pb^{2+} and different pH value of electrolyte solution at the preconcentration potential −0.6 V, frequency 15 Hz and amplitude 25 mV. From Fig. 5a, the peak current response of the constructed sensor increased rapidly with the augmentation of accumulation time for Pb^{2+} and achieved a maximum current at 250 s. Thus, an accumulation time of 250 s was selected as the experimental accumulation time for Pb^{2+}. In order to evaluate the effect of pH for the analytical Pb^{2+}, different pH values of the electrolyte in the pH range of 3.0–7.0 were researched. The experimental results were displayed in Fig. 5b. In the pH range of 3.0–4.0, the current values had a trend of slow growth. However, a sharp increase of the peak current value appeared in the pH range from 4.0 to 5.0. The possible reason may be that the electrode surface is unstable in acidic environment, resulting in lower current corresponding to the decreasing of pH value. Possibly, the response current was decreased along with the increasing from pH 5 to pH 7 because of the gradual hydrolysis of partial Pb^{2+} with the increase of pH value.

3.6. Analytical performance

Under the optimal conditions, SWVs were used to study the electrochemical responses of different concentrations Pb^{2+} on the L-Cys/NN-CuO/N-rGO/CPE in 0.1 M KNO_3 (pH 5.0) at the preconcentration time 250 s and potential −0.6 V, frequency 15 Hz and amplitude 25 mV. As can be seen in Fig. 6, the SWVs peak current gradually increasing accompanied with the enhancement of Pb^{2+} concentration. Moreover, the peak currents are linear with the Pb^{2+} concentration in the ranges of

Table 1 Comparison of different materials for the electrochemical detection of Pb^{2+}

Electrode materials	Detection limit (μM)	Linear range (μM)	References
CNT/rGO/Bi	0.00097	0.097–0.97	19
Hemin/G-quadruplex nanowires	1×10^{-9}	1×10^{-8} to 0.2	20
Pb^{2+}-Dependent DNAzyme/gold nanoparticles@Fe_3O_4	3×10^{-5}	0.0001–0.1	21
N-BDMP/Fe_3O_4/IL	0.0009	1.20–0.120	22
Sb_2O_3/MWCNTs	0.013	0.024–0.169	23
MOF-177	0.003	10–120	24
Evertically aligned MoS_2 nanofilm	0.001	0–0.097	25
Fe_3O_4/GN/GE	4.1×10^{-7}	1×10^{-6} to 0.0005; 0.0005–1	26
Bismuth–graphene	1.9×10^{-4}	4.8×10^{-4} to 0.2413	27
L-Cys/NN-CuO/N-rGO	8.0×10^{-8}	1×10^{-6} to 0.005; 0.005–1	This work

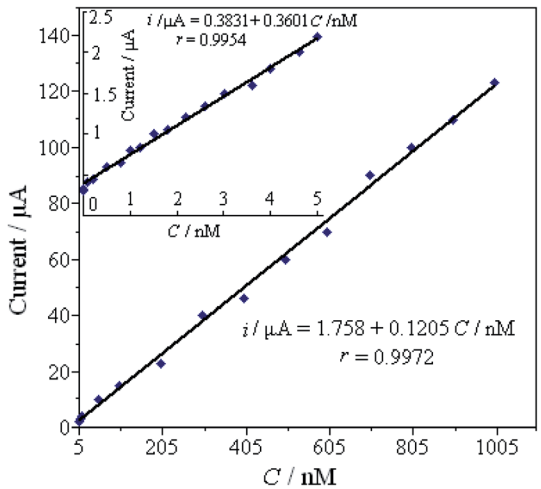

Fig. 7 The linear relationship of the peak current against the concentration of Pb^{2+} in the higher range of 5.0–1000 nM; the inset is the linear relationship between the current and concentration of Pb^{2+} in the lower range of 0.001–5.0 nM.

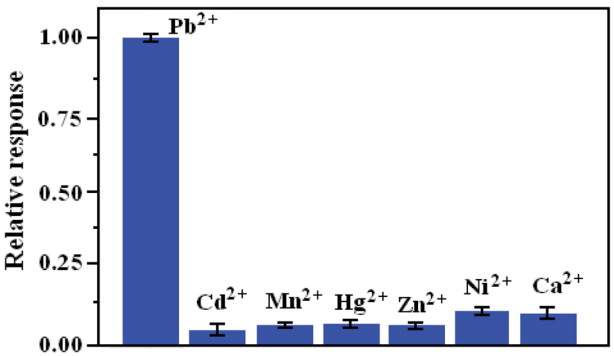

Fig. 8 Effect of the relative current response of 1.0 μM Pb^{2+} on L-Cys/NN-CuO/N-rGO/CPE. Error bars represent standard deviation, $n = 3$.

0.001–5.0 nM and 5.0–1000 nM, respectively (as displayed in Fig. 7). The limit of detection (LOD) of Pb^{2+} (S/N = 3) on the biosensor was determined to be 8.0×10^{-5} nM. Table 1 shows the comparative characteristics of the proposed sensor with some other reported sensors for the measurement of Pb^{2+}. The low detection limit of Pb^{2+} (8.0×10^{-5} nM) is lower than some other reported Pb^{2+} sensor,[21,23–29] except hemin/G-quadruplex bimolecular-based Pb^{2+} biosensors.[22] Comparing with the other reported different materials-modified sensors for Pb^{2+} detection, the as-constructed novel biosensor showed excellent capability for Pb^{2+} detection, such as lower detectable concentration, broader working range, and sensitivity. And more importantly, the developed biosensor has merits in preparation, for instance, a simple and convenient hydrothermal method without any surfactants or templates, cheapness with the employment of the natural substance L-cysteine for Pb^{2+} specific binding, without the employment of biological DNA and enzyme, as well as environmentally friendly without any toxicant.

3.7. Reproducibility and stability

The reproducibility and stability of the biosensor are the very important properties in the actual applications. In our study, the reproducibility of the L-Cys/NN-CuO/N-rGO modified electrode was tested by measuring the stripping peak current of 1.0 μM Pb^{2+} in 0.1 M KNO_3 (pH 5.0) for five successive determinations. The average relative standard deviation (RSD) was 4.66% with the same constructed electrode. The long-time stability of the as-prepared sensor was explored in two weeks with an evaluation every three days. The prepared modified electrode was put into a fridge (4 °C) when it is not used. The stripping peak currents of Pb^{2+} at the L-Cys/NN-CuO/N-rGO modified CPE retained about 87% of its original signal. These experimental results showed that the reproducibility and stability of the improved sensor were acceptable.

3.8. Selectivity of the prepared electrode

The selectivity of the proposed biosensor is examined before it was used to analyze the actual samples. We investigated the coexistent interference ions, such as Cd^{2+}, Mn^{2+}, Zn^{2+}, Ni^{2+}, Hg^{2+} and Ca^{2+} to evaluate the specificity of the prepared biosensor. As can be seen from Fig. 8, the histograms reveal the changed current of the sensor after the detection for other coexisting metal ions. It is obvious that the current signal was

Table 2 Determination of Pb^{2+} recovery by the suggested biosensor in different water samples (nM)

Samples	Pb^{2+} added (nM)	Pb^{2+} found (nM)	Recovery (%)	RSD (%)
Tab water	0	0.0192 ± 0.0010	—	3.56
	100	96 ± 1.05	96 ± 1.1	5.27
	1000	969 ± 16.35	96.9 ± 1.6	4.10
Rain water	0	0.0899 ± 0.0123	—	2.85
	100	98 ± 1.61	98 ± 1.6	3.97
	1000	1000 ± 20.67	100.0 ± 2.1	3.84
River water	0	0.186 ± 0.051	—	2.97
	100	94 ± 1.94	94 ± 1.9	6.01
	1000	1006 ± 23.20	100.6 ± 2.3	4.32
Industrial effluent	0	0.271 ± 0.037	—	3.02
	100	103 ± 2.29	103 ± 2.3	4.17
	1000	1015 ± 35.71	101.5 ± 3.6	5.79

significantly larger with Pb^{2+} of 1.0 μM than those of other coexisting metal ions (1.0 μM). The experimental phenomena clearly proved that the proposed method could reasonable selectively determine Pb^{2+} in the presence of other interfering metal ions.

3.9. The practicality of the proposed sensor

To evaluate the practicality of the constructed method, standard addition recovery tests for tap water, rain water, and river water (river located in Anyang, China) were researched. Before testing, all samples were filtered through filter membrane to get rid of insoluble substance, and then adjust it to the optimized pH by 0.1 M KNO_3 and HNO_3. The detection results are listed in Table 2. As can be observed, the recoveries are ranged from 94% to 103%, and relative standard deviations (RSDs) are 2.85–6.01%, respectively, indicating that the proposed biosensor has a potential application in the specific detection of Pb^{2+} in real samples.

4. Conclusions

In conclusion, an effective method was proposed to measure Pb^{2+} by combining L-cysteine and NN-CuO/N-rGO as electrode materials. L-Cysteine, as the natural substance was used as specific receptor for Pb^{2+} analysis and NN-CuO/N-rGO nanocomposite as improved sensing material. The proposed biosensor displayed useful linear ranges, acceptable detection limit, high sensitivity and good selectivity for electrochemical detection of Pb^{2+}. This study indicates that the present L-Cys/NN-CuO/N-rGO/CPE provide a specific potential applications in the development of other nanodevices for metal ions detections.

Conflicts of interest

There are no conflicts to declare.

Acknowledgements

We acknowledge the financial support of the National Natural Science Foundation of China (21804002), the Program for Science and Technology Innovation Talents at the University of Henan Province (20HASTIT009), and Anyang Science and Technology Bureau (No. 28).

References

1 C. Jiang, Y. Li, H. Wang, D. Chen and Y. Wen, *Sens. Actuators, B*, 2020, **307**, 127625–127632.
2 Z. Yang, H. Wu, X. Yi, J. Tang, W. Yun, W. Han and X. Chen, *Biosens. Bioelectron.*, 2019, **144**, 111679–111688.
3 J. C. Meyer, A. K. Geim, M. I. Katsnelson, K. S. Novoselov, T. J. Booth and S. Roth, *Nature*, 2007, **446**, 60–63.
4 S. Taniselass, M. K. M. Arshad and S. C. B. Gopinath, *Biosens. Bioelectron.*, 2019, **130**, 276–292.
5 Y. Zuo, J. Xu, X. Zhu, X. Duan, L. Lu and Y. Yu, *Microchim. Acta*, 2019, **186**, 1–9.
6 S. Kim, K. C. Kwon, J. Y. Park, H. W. Cho, I. Lee, S. Y. Kim and J. L. Lee, *ACS Appl. Mater. Interfaces*, 2016, **8**, 12932–12939.
7 J. H. Kim, A. Mirzaei, Y. Zheng, J. H. Lee, J. Y. Kim, H. W. Kim and S. S. Kim, *Sens. Actuators, B*, 2019, **281**, 453–461.
8 Y. Li, X. Wang, Q. Yang, M. S. Javed, Q. Liu, W. Xu, C. Hu and D. Wei, *Electrochim. Acta*, 2017, **234**, 63–70.
9 Y. Xie, Y. Yu, L. Lu, X. Ma, L. Gong, X. Huang, G. Liu and Y. Yu, *J. Electroanal. Chem.*, 2018, **812**, 82–89.
10 Y. Liu, M. Li, H. Li, G. Wang, Y. Long, A. Li and B. Yang, *ACS Sustainable Chem. Eng.*, 2019, **7**, 19537–19545.
11 F. Faranak, R. Mansour, H. Mohammad Jafar and K. Hasuck, *Microchim. Acta*, 2018, **185**, 57–66.
12 D. Majumdar, N. Baugh and S. K. Bhattacharya, *Colloids Surf., A*, 2017, **512**, 158–170.
13 S. Felix, X. Charles and A. N. Grace, *Sens. Lett.*, 2017, **15**, 60–64.
14 X. Wang, J. Hao, J. Cheng, J. Li, J. Miao, R. Li, Y. Li, J. Li, Y. Liu, X. Zhu, Y. Liu, X. W. Sun, Z. Tang, M. H. Delville, T. He and R. C. Chiral, *Nanoscale*, 2019, **11**, 9327–9334.
15 Y. Cheng, H. Fa, W. Yin, C. Hou, D. Huo and F. Liu, *J. Solid State Electrochem.*, 2015, **20**, 327–335.
16 W. Zhou, C. Li, C. Sun and Y. Yang, *Food Chem.*, 2016, **192**, 351–357.
17 S. L. Yang, G. Li, D. Wang, Z. Qiao and L. B. Qu, *Sens. Actuators, B*, 2017, **238**, 588–595.
18 B. R. LyrioFerraz, F. R. F. Leite and A. R. Malagutti, *Talanta*, 2016, **154**, 197–207.
19 Q. Xu and S. F. Wang, *Microchim. Acta*, 2005, **151**, 47–52.
20 B. Rezaei and S. Z. Mirahmadi Zare, *Sens. Actuators, B*, 2008, **134**, 292–299.
21 X. Xuan and J. Y. Park, *Sens. Actuators, B*, 2018, **255**, 1220–1227.
22 M. Qing, Y. Yuan, W. Cai, S. Xie and J. Zhang, *Sens. Actuators, B*, 2018, **263**, 469–475.
23 L. Zhang, H. Deng, R. Yuan and Y. Yuan, *Mikrochim. Acta*, 2019, **186**, 709–718.
24 I. Vida, R. Mosayeb and M. Jafar, *Anal. Bioanal. Chem. Res.*, 2019, **6**, 405–417.
25 T. L. Hai, L. C. Hung, T. T. B. Phuong, B. T. T. Ha, B. S. Nguyen, T. D. Hai and V. H. Nguyen, *Microchem. J.*, 2020, **153**, 104456–104464.
26 S. Sangeetha and G. Krishnamurthy, *Bull. Mater. Sci.*, 2020, **43**, 29–37.
27 J. H. Hwang, M. A. Islam, H. Choi, T. J. Ko, K. L. Rodriguez, H. S. Chung, Y. Jung and W. Hyoung Lee, *Anal. Chem.*, 2019, **91**, 11770–11777.
28 B. He, X. F. Shen, J. Nie, X. L. Wang, F. M. Liu, W. Yin, C. J. Hou, D. Q. Huo and H. B. Fa, *J. Solid State Electrochem.*, 2018, **22**, 3515–3525.
29 W. Wonsawat, S. Chuanuwatanakul, W. Dungchai, E. Punrat, S. Motomizu and O. Chailapakul, *Talanta*, 2012, **100**, 282–289.

